Journal of Applied Geophysics 155 (2018) 256–264

Contents lists available at ScienceDirect

Journal of Applied Geophysics

journal homepage: www.elsevier.com/locate/jappgeo

Up- and downgoing borehole wavefield retrieval using single component borehole and reflection data

Yi Liu [a,*], Børge Arntsen [b], Joost van der Neut [c], Kees Wapenaar [c]

[a] Department of Electronic Systems, Norwegian University of Science and Technology, 7491 Trondheim, Norway
[b] Department of Geoscience and Petroleum, Norwegian University of Science and Technology, 7491 Trondheim, Norway
[c] Department of Geoscience and Engineering, Delft University of Technology, 2628CN Delft, the Netherlands

ARTICLE INFO

Article history:
Received 24 October 2017
Received in revised form 29 May 2018
Accepted 3 June 2018
Available online xxxx

ABSTRACT

A standard procedure in processing vertical seismic profile (VSP) data is the separation of up- and downgoing wavefields. We show that these wavefields in boreholes can be retrieved using only single-component data, given that a full set of surface reflection data is also available. No medium parameters are required. The method is an application of the Marchenko method and uses a focusing wavefield. It is a wavefield that satisfies certain focusing conditions in a reference medium. We show that the method is applicable to boreholes with any orientation, and no receiver array is required. By this work, we present two contributions. One is that we investigate the effect of using only the traveltime from borehole data to form the focusing wavefield. The second is that we validates standard separation methods (PZ summation and *f-k* filtering) by retrieving the one-way wavefields from a completely different approach. We use the numerically modelled data from a realistic field velocity model in the North Sea. Three borehole geometries (horizontal, deviated and vertical) are tested. We discuss the practical aspects for field application in the end.

1. Introduction

Seismic data acquired in boreholes have long been used in aiding the geological interpretation of the subsurface. For vertical wells, these data are called vertical seismic profiles (VSP). VSP data are useful for identification and confirmation of the events seen on surface seismic data, seismic-stratigraphic analysis, seismic velocity analysis and calibration, imaging and time-lapse reservoir monitoring, and predicting ahead of the drill bit (Hardage, 1985; Poletto et al., 2004). Overviews of conventional VSP processing techniques and successful field examples can be found in Kennett et al. (1980) and Balch et al. (1982).

Due to its acquisition geometry, an important VSP processing step is the separation of the up- and downgoing fields. Conventional VSP up-down separation methods are based on the separation of different apparent velocities (or dips) of the up- and downgoing fields. Generally speaking, upgoing events have positive dips and downgoing events have negative dips. Velocity filters are commonly used to separate them in the frequency-wavenumber (*f-k*) domain (Embree et al., 1963; Treitel et al., 1967). Besides the separation in the *f-k* domain, separation in the τ-p domain after applying Radon transform is suggested by Moon et al. (1986). In this approach, the up-down components are mapped to different τ-p quadrants according to their dips so that they can be separated. This technique is useful when the separation is difficult in the *f-k* domain.

With the availability of multi-component data, more sophisticated wave-equation based decomposition methods are developed. Dankbaar (1985) proposes a decomposition scheme which uses weighted summations of vertical and horizontal geophone measurements in the *f-k* domain. Wapenaar et al. (1990) present a scheme to decompose land surface data into up-downgoing P- and S-waves. Other separation methods that are based on eigenvalue decomposition of the equation of motion with certain boundary conditions in horizontally-layered media. Ursin (1983) show that the up- and downgoing fields can be computed as an angle-dependent combination of two or more measured data components. Barr and Sanders (1989) show the use of a scalar combination of the hydrophone (pressure) and vertical geophone (particle velocity) measurements to suppress water-column reverberations. This approach is commonly referred to as PZ summation. It is simple to implement but valid for normal incidence only. An angle-dependent decomposition for multi-component sea-floor data is proposed by Amundsen (1993) and Amundsen and Reitan (1995), which requires the seabed velocity and density. Schalkwijk et al. (2003) propose a 5-step adaptive decomposition scheme that obtains the necessary information from data, and it is further extended by Muijs et al. (2004) to be applied in an efficient automated manner.

In this paper, we show another approach that is also wave-equation based, but retrieves the up- and downgoing fields in boreholes using

* Corresponding author.
E-mail address: yi.liu@ntnu.no (Y. Liu).

https://doi.org/10.1016/j.jappgeo.2018.06.003
0926-9851/

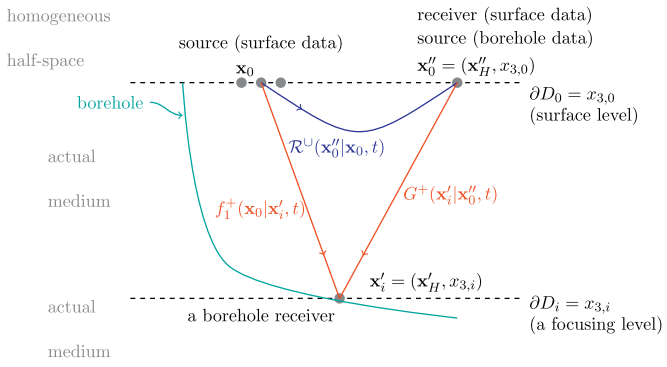

Fig. 1. Notation convention and data acquisition overview. Each spatial position is denoted by $(\mathbf{x}_H, x_{3,i})$, with $\mathbf{x}_H = (x_1, x_2)$, and i represents a certain depth level. The upper dashed line denotes a transparent surface level ∂D_0, above which the medium is homogeneous, and the lower dashed line denotes a focusing level ∂D_i (below which the medium is reflection-free for the focusing function, see Fig. 2). The solid blue line represents the known surface reflection response $R^{\cup}(\mathbf{x}_0''|\mathbf{x}_0, t)$ after source deconvolution and surface multiple removal. The solid red lines represent the unknown quantities, where $f_1^+(\mathbf{x}_0|\mathbf{x}_i', t)$ is the downgoing component of the focusing function with the focus position $\mathbf{x}_i'$ and $G^+(\mathbf{x}_i'|\mathbf{x}_0'', t)$ is the retrieved downgoing wavefield from a surface source at $\mathbf{x}_0''$. Note that G^+ additionally contains the interaction with the medium below the focusing level. For f_1^+, the medium below the focusing level is homogenous and not the actual medium. (For interpretation of the references to colour in this figure legend, the reader is referred to the web version of this article.)

only the acoustic pressure data recorded at the surface and in the borehole. The method is valid for a general lossless inhomogeneous medium with moderately curved interfaces. It accounts for all internal multiples and is not limited to normal incidence. No medium parameters are required, and it can be used for a single borehole receiver (an array of receivers is not needed). The method uses the so-called focusing wavefields from the Marchenko method (Rose, 2002; Broggini et al., 2012; Wapenaar et al., 2013; Behura et al., 2014), which are computed from surface reflection data and borehole data. From these focusing functions, one is able to retrieve at a borehole receiver, the up- and downgoing wavefields. We show that the method works for any general borehole orientation, and its results agree with those by other methods. This approach is tested with synthetic data, modelled for a density and velocity model realistic for North Sea. Three borehole geometries are included, namely, horizontal, deviated, and vertical. The retrieved up- and downgoing fields are compared with those by conventional methods in each case. In the horizontal configuration, we also investigate the effect from a less-than-ideal initial focusing wavefield, where only the smoothed traveltime from borehole data is used. We then discuss these results and their applicability to field data.

2. Method

The Marchenko method (Wapenaar et al., 2014) is able to retrieve up- and downgoing subsurface wavefields from surface sources. It

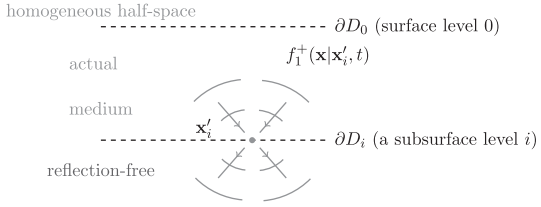

Fig. 2. An illustration of the downgoing focusing wavefield $f_1^+(\mathbf{x}|\mathbf{x}_i', t)$. After being injected at the surface level ∂D_0 at $t = -t_d(\mathbf{x}_0|\mathbf{x}_i')$, it propagates downward and focuses at $\mathbf{x}_i'$ at $t = 0$. $t_d(\mathbf{x}|\mathbf{x}_i')$ is the direct travel time from $\mathbf{x}_0$ to $\mathbf{x}_i'$. Then the wavefield continues propagating downward from the level i. Notice that the medium below that level is defined as reflection-free, which is different from that in Fig. 1, where the retrieved G^+ additionally contains the interaction with the medium below the focusing level.

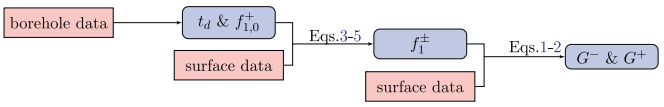

Fig. 3. The general workflow for retrieving the up- and downgoing fields. The red boxes denote the input data, and the round-cornered purple boxes denote the computed results. (For interpretation of the references to colour in this figure legend, the reader is referred to the web version of this article.)

requires surface reflection responses and the direct wavefield from the subsurface location to the surface source positions, which can be obtained from a smooth background velocity model. However, velocity

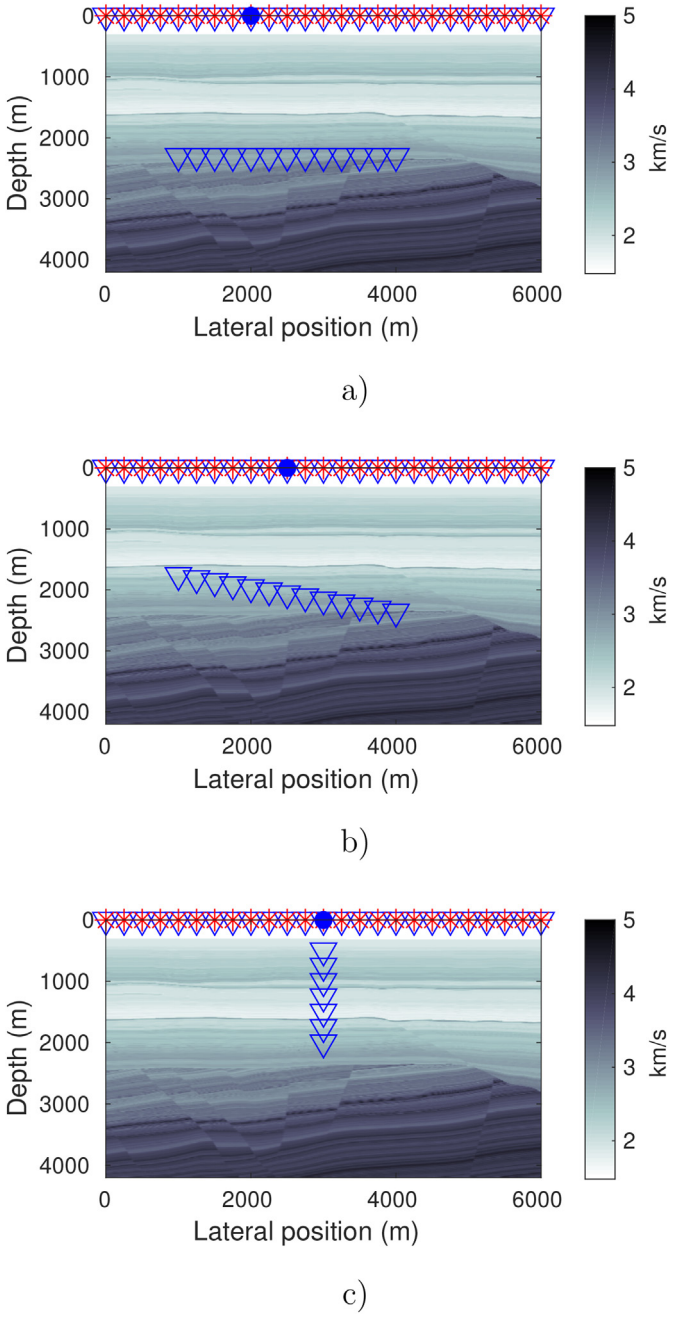

Fig. 4. The P-wave velocity model and the acquisition geometries for the a) horizontal borehole, b) deviated borehole and c) vertical borehole. The stars denote the sources in both the surface and borehole data, and the triangles denote the receivers. The blue circles denote the reference source positions, where the retrieved one-way wavefields are shown. (For interpretation of the references to colour in this figure legend, the reader is referred to the web version of this article.)

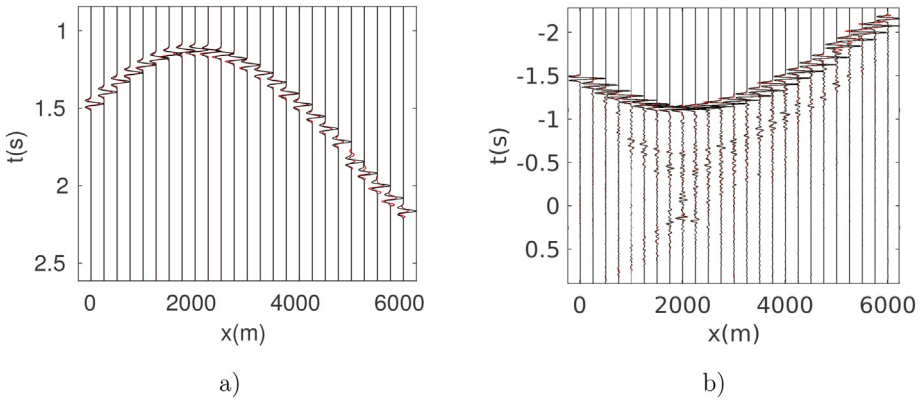

Fig. 5. An example of a) the direct wavefield in borehole data and b) the corresponding downgoing focusing wavefield f_1^+, computed using the iterative Marchenko method. The focusing positions are at a lateral position of 2 km. The actual direct field is shown in red and the synthetic one created by convolving the smoothed traveltime curve with a Ricker wavelet is shown in black. (For interpretation of the references to colour in this figure legend, the reader is referred to the web version of this article.)

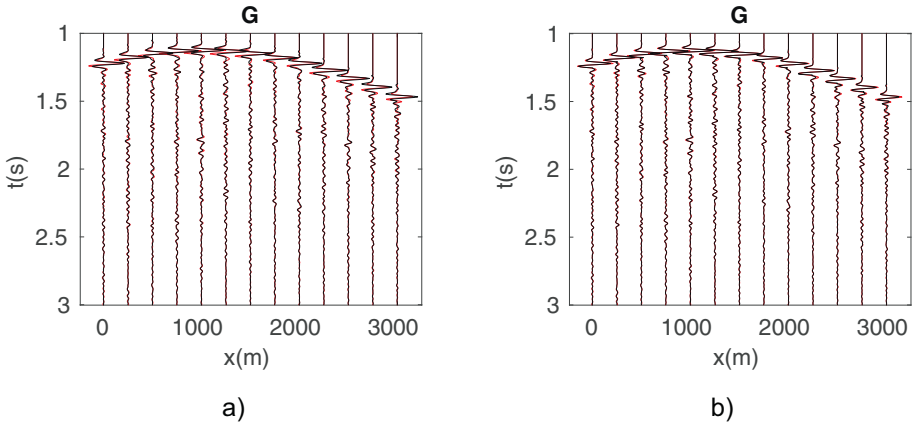

Fig. 6. Horizontal borehole case. The common-source comparison of the retrieved total wavefield ($U + D$, in black) and the recorded pressure wavefield (in red). a) is retrieved by using the synthetic less-than-ideal initial focusing wavefield, as shown by the black traces in Fig. 5. b) is retrieved by using the correct direct wavefield from borehole. Every tenth trace is plotted. (For interpretation of the references to colour in this figure legend, the reader is referred to the web version of this article.)

models are not always available, and even when they are, an inaccurate velocity model can affect the retrieved results depending on the velocity error (Thorbecke et al., 2013; de Ridder et al., 2016). Borehole data, on the other hand, provides exact traveltimes. Thus it enables a more accurate and velocity-free Marchenko scheme, which in turn provides the sought-after up- and downgoing separated borehole wavefields.

2.1. The up-down wavefield retrieval

First, we introduce Fig. 1 for the notation and the data geometries. A spatial position is denoted as $\mathbf{x}_i = (\mathbf{x}_H, x_{3,\,i})$, where $\mathbf{x}_H = (x_1, x_2)$ represents the horizontal position and $x_{3,\,i}$ represents the depth level. For example, $\mathbf{x}_0''$ represents a position at a lateral coordinate $\mathbf{x}_H''$ at the surface

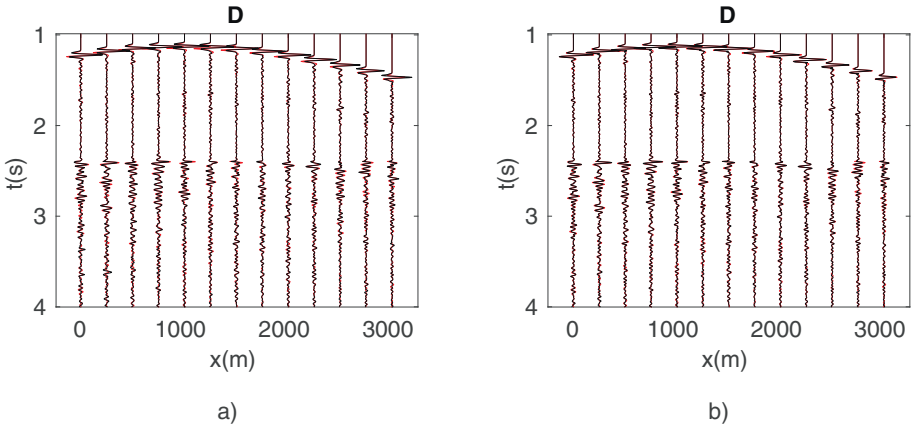

Fig. 7. Horizontal borehole case. The common-source comparison of the retrieved downgoing wavefield (in black) and the result by a standard PZ summation (in red) method. a) is retrieved by using the less-than-ideal initial focusing wavefield. b) is retrieved by using the correct direct wavefield from borehole. The events after the direct arrivals in the downgoing field is scaled up by a factor of 6 for viewing. (For interpretation of the references to colour in this figure legend, the reader is referred to the web version of this article.)

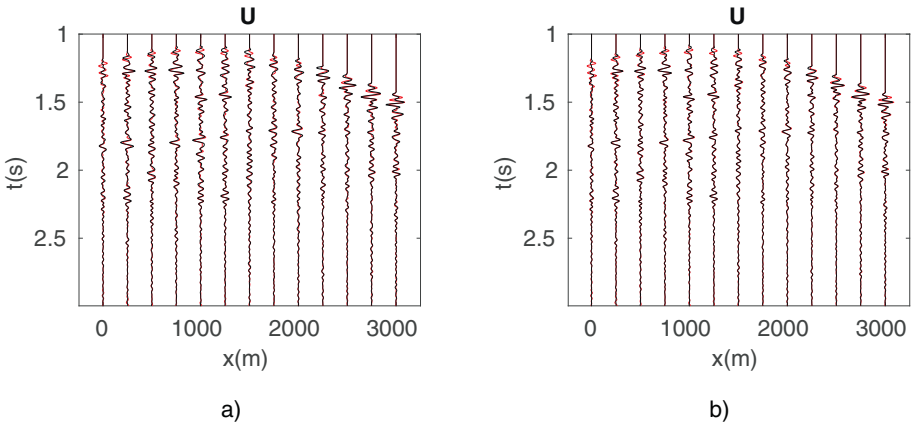

Fig. 8. Horizontal borehole case. The same comparison as in Fig. 7, but for the upgoing wavefield.

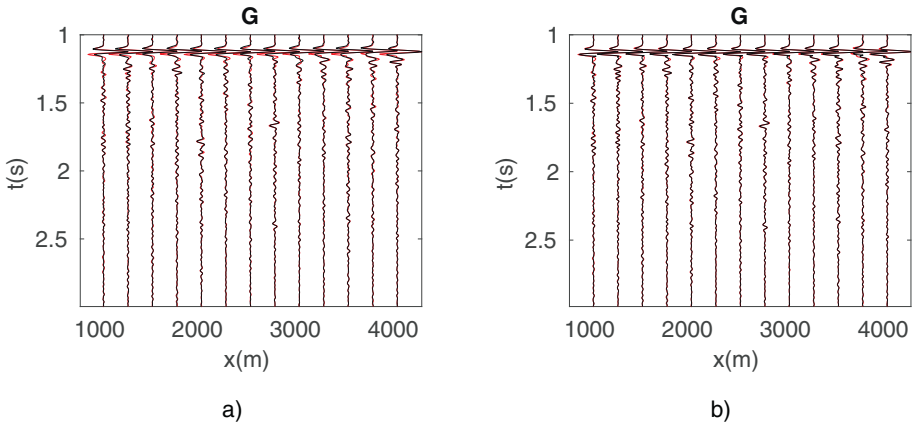

Fig. 9. Horizontal borehole case. The zero-offset comparison of the retrieved total wavefield ($U + D$, in black) and the recorded pressure wavefield (in red) in borehole. a) is retrieved by using the synthetic less-than-ideal initial focusing wavefield, as shown by the black traces in Fig. 5. b) is retrieved by using the correct direct wavefield from borehole. (For interpretation of the references to colour in this figure legend, the reader is referred to the web version of this article.)

level ∂D_0, and similarly, $\mathbf{x}_i'$ represents a position at a lateral coordinate $\mathbf{x}_H'$ at a subsurface level ∂D_i. The surface level ∂D_0 is defined as a transparent boundary, indicated by the upper dashed line in Fig. 1, so the free surface reflections are excluded. The green line shows a general borehole, and each borehole receiver position is denoted as $\mathbf{x}_i$, where i may vary according to the depth. In other words, the borehole need not be horizontal. The blue colour indicates the known surface reflection response $R^{U}(\mathbf{x}_0''|\mathbf{x}_0, t)$ recorded at $\mathbf{x}_0''$ from a source at $\mathbf{x}_0$. The red colour indicates two of the unknown quantities, the downgoing components of the focusing function $f_1^+(\mathbf{x}_0|\mathbf{x}_i', t)$ and of the pressure wavefield $G^+(\mathbf{x}_i'|\mathbf{x}_0'', t)$. More on the focusing functions will be explained, but first, the relation between the blue and the red quantities is the following (Wapenaar et al., 2014).

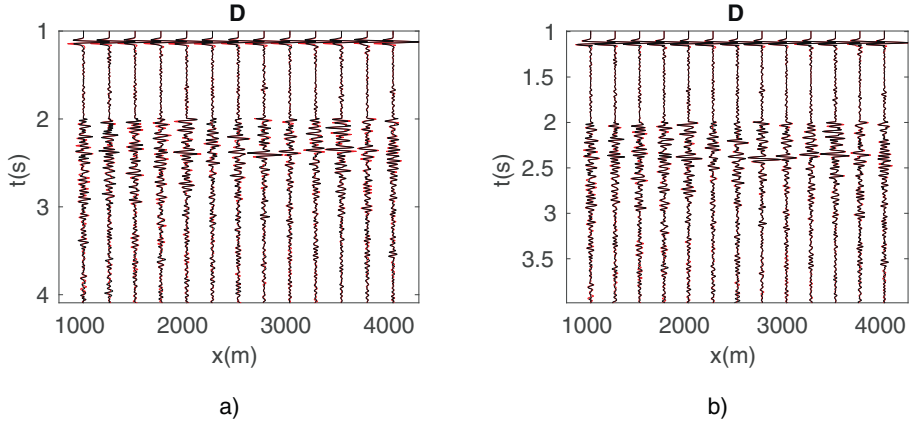

Fig. 10. Horizontal borehole case. The zero-offset comparison of the retrieved downgoing wavefield (in black) and the result by a standard PZ summation (in red) method. The events after the direct arrivals in the downgoing field is scaled up by a factor of 8 for viewing. (For interpretation of the references to colour in this figure legend, the reader is referred to the web version of this article.)

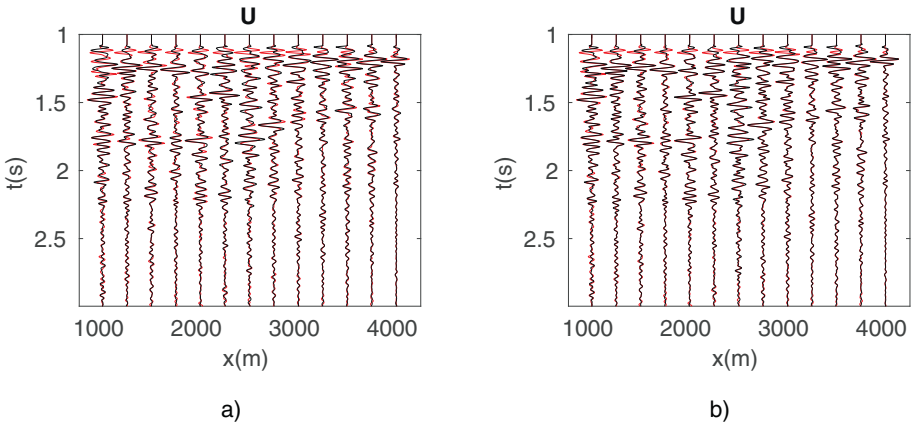

Fig. 11. Horizontal borehole case. The same comparison as in Fig. 10, but for the upgoing wavefield.

For $t \geq t_d(\mathbf{x}_0''|\mathbf{x}_i')$ (the direct travel time from a position $\mathbf{x}_i'$ in the borehole to a position $\mathbf{x}_0''$ at the surface), the up- and downgoing fields can be computed by

$$G^{-}(\mathbf{x}_i'|\mathbf{x}_0'', t) = \int_{\partial D_0}\int_{-\infty}^{t} R^{\cup}(\mathbf{x}_0''|\mathbf{x}_0, t-t') f_1^{+}(\mathbf{x}_0|\mathbf{x}_i', t')\, dt'\, d\mathbf{x}_0 \tag{1}$$

and

$$G^{+}(\mathbf{x}_i'|\mathbf{x}_0'', t) = f_{1,0}^{+}(\mathbf{x}_0''|\mathbf{x}_i', -t) - \int_{\partial D_0}\int_{-\infty}^{t} R^{\cup}(\mathbf{x}_0''|\mathbf{x}_0, t-t') f_1^{-}(\mathbf{x}_0|\mathbf{x}_i', -t')\, dt'\, d\mathbf{x}_0. \tag{2}$$

here $R^{\cup}(\mathbf{x}_0''|\mathbf{x}_0, t)$ is the known surface reflection response after surface mulitple elimination, deghosting and the deconvolution of the wavelet, the same definition as in Wapenaar et al. (2014) and Thorbecke et al. (2017). And $f_1^{\pm}(\mathbf{x}_0|\mathbf{x}_i', t)$ are the one-way focusing functions to be found by an iterative Marchenko scheme (shown below), and $G^{\pm}(\mathbf{x}_i'|\mathbf{x}_0'', t)$ are the up- and downgoing components of the band-limited Green's functions. The subscript 0 in $f_{1,0}^{+}$ stands for the initial estimate of f_1^{+}.

In order to use these two equations, one needs to find the focusing functions $f_1^{\pm}(\mathbf{x}_0|\mathbf{x}_i', t)$, whose sum describes a pressure wavefield that satisfies the wave equation in the medium between ∂D_0 and ∂D_i and focuses at the focusing position $\mathbf{x}_i'$ at $t = 0$. An illustration of its downgoing component is shown in Fig. 2, and an exact description of the focusing condition can be found in Wapenaar et al. (2014).

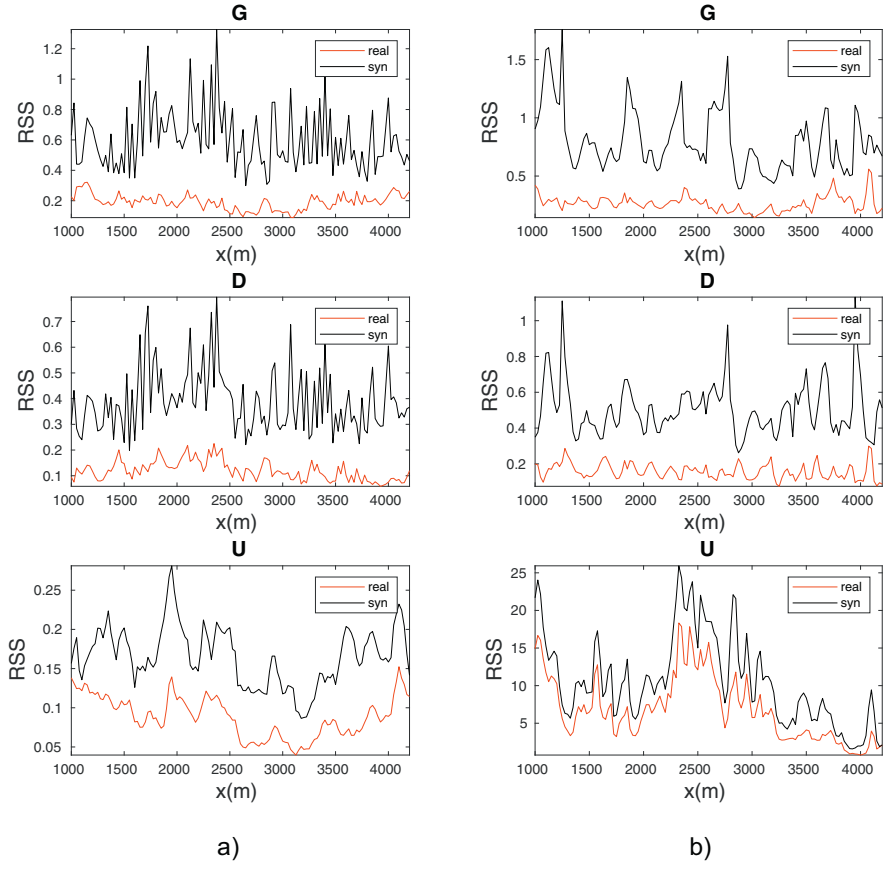

Fig. 12. Residual sum of squares of the amplitude for a) the common-source results, and b) the zero-offset results. It confirms that the use of the recorded direct wavefield is better than using only the traveltime. It also reveals that impact of the synthetic direct wavefield is mainly on the downgoing wavefield rather than the upgoing wavefield.

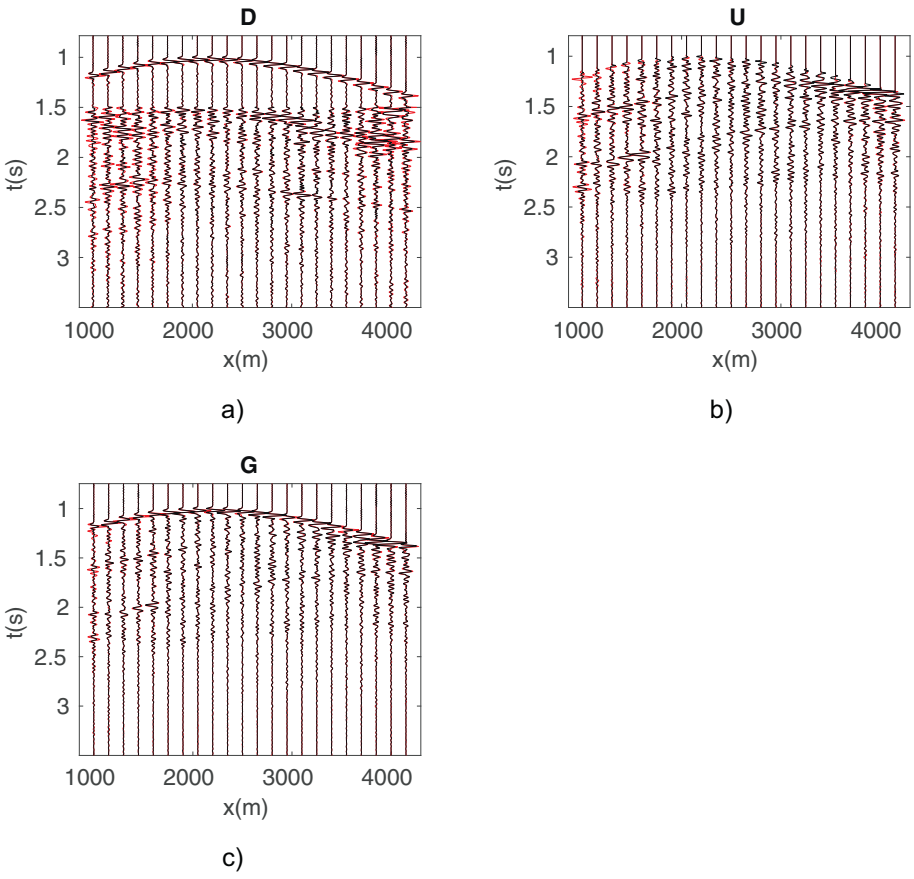

Fig. 13. Deviated borehole case. The common-source comparison of the retrieved wavefields (in black) and the reference wavefield (in red). The source position is at 2500 m at the surface. a) The downgoing and b) the upgoing wavefields. A standard PZ summation is used. The events after 1.5 s in the downgoing waves are scaled up by a factor of 8 for viewing. Every sixth trace is plotted. c) The retrieved total wavefield ($U + D$, in black) is compared to the recorded pressure wavefield (in red) in borehole. (For interpretation of the references to colour in this figure legend, the reader is referred to the web version of this article.)

These focusing functions $f_1^{\pm}(\mathbf{x}_0|\mathbf{x}_i{}'_{iiiii},t)$ are found by an iterative Marchenko scheme, starting with an initial estimate of $f_1^{+}(\mathbf{x}_0|\mathbf{x}_i{}',t)$. More details on the Marchenko scheme, the focusing functions and its implementation are explained by Wapenaar et al. (2013, 2014); Slob et al. (2014) and Thorbecke et al. (2017). Here we summarise the scheme with Eqs. (3) to (5), which read

$$f^{+}_{1,k}(\mathbf{x}_0^{''}|\mathbf{x}_i',t) = f^{+}_{1,0}(\mathbf{x}_0^{''}|\mathbf{x}_i',t) + \theta(t+t_d(\mathbf{x}_0^{''}|\mathbf{x}_i'))\int_{\partial D_0}\int_{-\infty}^{\infty} R^{U}(\mathbf{x}_0^{''}|\mathbf{x}_0',t')f^{-}_{1,k-1}(\mathbf{x}_0'|\mathbf{x}_i',t+t')dt'd\mathbf{x}_{0'} \tag{3}$$

$$f^{-}_{1,k}(\mathbf{x}_0^{''}|\mathbf{x}_i',t) = \theta(t_d(\mathbf{x}_0^{''}|\mathbf{x}_i')-t)\int_{\partial D_0}\int_{-\infty}^{\infty} R^{U}(\mathbf{x}_0^{''}|\mathbf{x}_0',t-t')f^{+}_{1,k}(\mathbf{x}_0'|\mathbf{x}_i',t')dt'd\mathbf{x}_{0'} \tag{4}$$

with

$$f^{+}_{1,0}(\mathbf{x}_0^{''}|\mathbf{x}_i',t) \approx G_d(\mathbf{x}_i'|\mathbf{x}_0^{''},-t) \tag{5}$$

where $\theta(t)$ is the Heaviside function, and k is iteration number starting from 0. For simplicity, we use the time reversal of the direct arrival in Eq. (5) as an approximation. The technically correct term is the direct arrival of the inverse transmission response (Wapenaar et al., 2014). First, by setting $k = 0$ in Eq. (5), one forms the first estimate of $f^{+}_{1,0}$ according to Eq. (4) by using the time-reversed direct wavefield from $\mathbf{x}_0$ to $\mathbf{x}_i'$ in the borehole data as $G_d(\mathbf{x}_i'|\mathbf{x}_0,-t)$. By setting $k = 1$, the first update $f^{+}_{1,1}$ can be computed from Eq. (3), and subsequently the upgoing component $f^{-}_{1,1}$ from Eq. 4. After repeating the procedure for a few iterations until converged $f_1^{\pm}$ are found, it can then be substituted back into Eqs. 1 and 2 for the up- and downgoing fields. In this last step, again, only the surface reflection data and the direct wavefield travel times are needed. An overall processing flow chart is shown in Fig. 3.

3. Numerical results

The synthetic data are modelled using a realistic P-wave velocity model from the North Sea. To show that the method is not limited to any particular borehole orientation, three borehole geometries (horizontal, deviated and vertical) are used. Fig. 4 shows the model and the data geometries. In all three cases, there are 241 sources and receivers in the surface reflection data, with a source / receiver spacing of 25 m. A finite difference method (Thorbecke and Draganov, 2011) is used for generating the synthetic acoustic pressure datasets. The source signal in the surface data is a band-limited delta function with a maximum frequency of 55 Hz. The free surface related multiples are not included in the modelling, which is an ideal scenario for the method. The source signal for the borehole data is a Ricker wavelet with a peak frequency of 15 Hz.

3.1. Horizontal borehole

In this case, there are 129 receivers in the borehole of the depth 2.3 km, starting from $x_1 = 1000$ m to $x_1 = 4200$ m, with a spacing of 25 m, as shown in Fig. 4a. The source positions for the borehole data are the same as in the surface data.

One way to form the initial estimate of the focusing wavefield is time windowing the direct wavefield in the borehole data, as this preserves

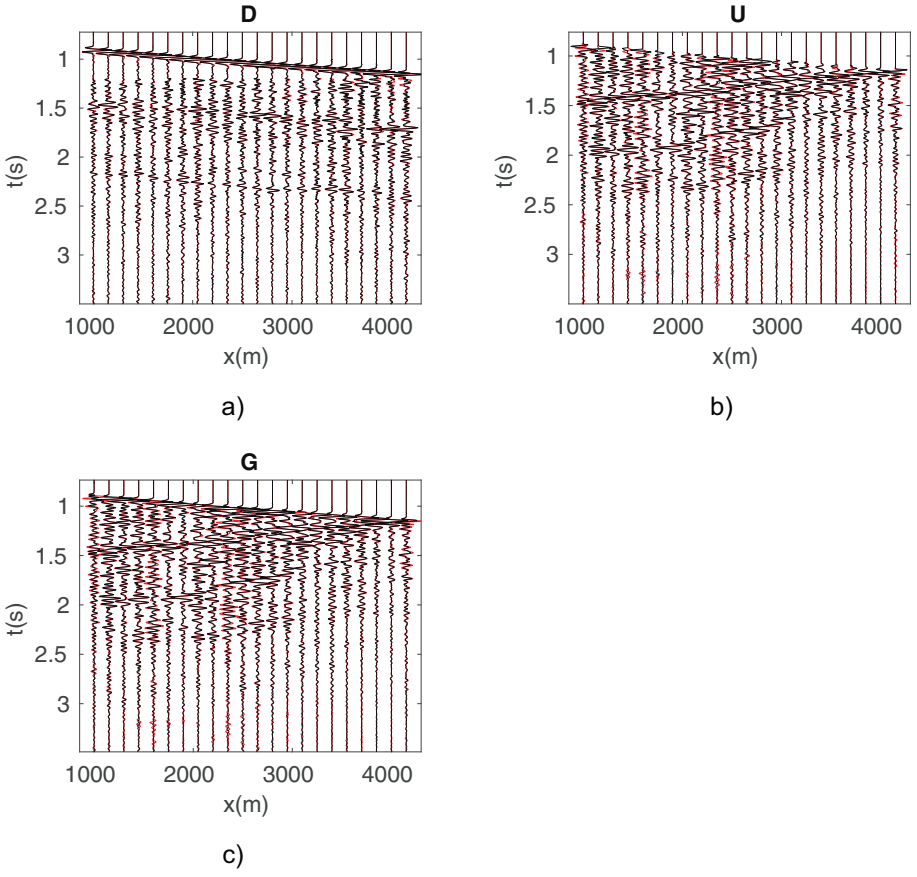

Fig. 14. Deviated borehole case. The zero-lateral-offset comparison of the retrieved wavefields (in black) and the reference wavefield (in red). The source position is at 2500 m at the surface. a) The downgoing and b) the upgoing wavefields. A standard PZ summation is used. The events after 1.5 s in the downgoing waves are scaled up by a factor of 8 for viewing. Every sixth trace is plotted. c) The retrieved total wavefield ($U + D$, in black) is compared to the recorded pressure wavefield (in red) in borehole. (For interpretation of the references to colour in this figure legend, the reader is referred to the web version of this article.)

the correct amplitude. However, time windowing may not work for large far-offsets due to the head waves, etc.. Therefore, to study the method's sensitivity to such effect, we repeat the same workflow to retrieve the up- and downgoing field, one with the correct direct wavefield, and one with the synthetic direct wavefield.

To form this synthetic direct wavefield, we extract the traveltime curves with the maximum amplitude, make sure it is a smooth curve and then convolve it with a zero-phase wavelet. It alters what should be the inverse of the direct wavefield, and we will see how it affects the retrieved up- and downgoing fields. The comparison of the two initial direct fields are shown in Fig. 5a and the corresponding focusing wavefields in Fig. 5b.

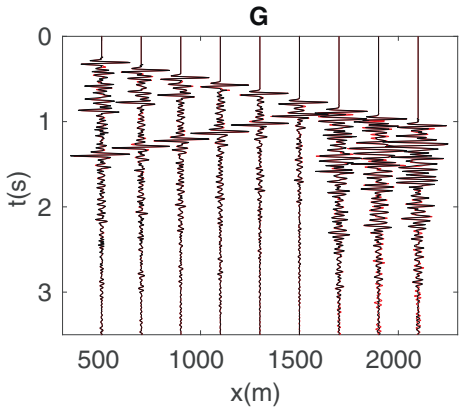

Fig. 15. Vertical borehole case. The comparison of the retrieved total wavefield ($U + D$, in black) and the recorded pressure field (in red) in borehole. (For interpretation of the references to colour in this figure legend, the reader is referred to the web version of this article.)

Fig. 6 is the common-source comparison of the retrieved total response G (in black) with those by an angle-dependent PZ summation method (in red). The up- and downgoing fields are shown in Figs. 7 and 8. In Fig. 7 for the downgoing field, the events after the direct arrivals are gained by a factor of 8 for viewing. This factor is chosen by trial and error to achieve a suitable visual result. For this trace-by-trace comparison, an overall scaling factor is used, where the maximum amplitude in the retrieved downgoing wavefield is scaled with that in the measured borehole data. This does not alter the amplitude-versus-offset behaviour in the retrieved wavefields.

Overall, the figures show that this method gives similar results as the standard PZ summation approach. Secondly, we can see that this less-than-ideal initial direct wavefield does have an effect on the results, but only to a limited degree. The kinematics in the retrieved results are not affected by this erroneous input. The similar comparison, but for the zero-offsets are shown in Figs. 9, 10 and 11. To have a clearer overview of the error from the synthetic initial input, the residual sum of squares (RSS) of the amplitude for the common-source and zero-offset comparisons are plotted in Fig. 12. It confirms that amplitude error is smaller using the actual direct wavefield than using only the traveltime. It also shows that this incorrect direct wavefield mainly affects the downgoing wavefield rather than the upgoing wavefield. In the next two examples, the deviated and vertical ones, we will use only the correct direct wavefield as the initial focusing wavefield.

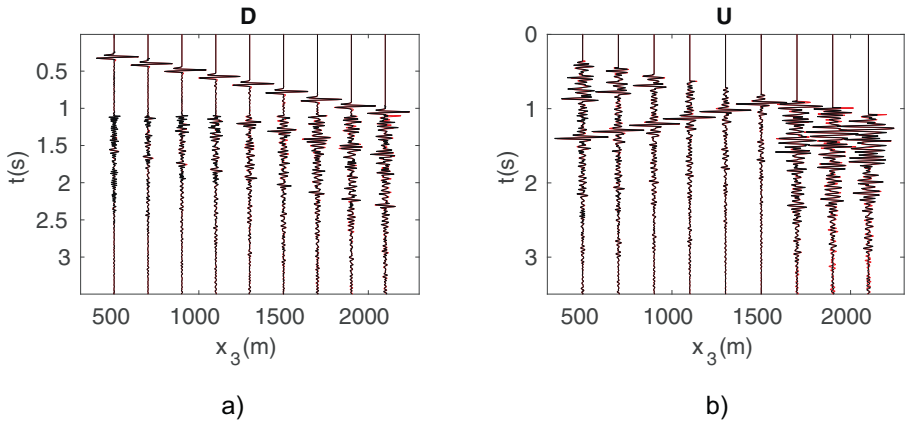

Fig. 16. Vertical borehole case. The comparison of the retrieved wavefields (in black) of a source at $x_1 = 3000$ m at the surface. They are compared to those by standard PZ summation (in red). a) The downgoing field. An amplitude gain of a factor of 8 is applied on the events after the direct arrivals. b) The upgoing field. Every sixth trace is plotted. (For interpretation of the references to colour in this figure legend, the reader is referred to the web version of this article.)

3.2. Deviated borehole

In the deviated borehole case, there are 129 receivers in the borehole. The lateral position of the borehole receivers is from $x_1 = 1000$ m to $x_1 = 4200$ m with a 25 m interval. The depth of the receivers is from $x_3 = 1760$ m to $x_3 = 2400$ m with a 5 m interval. The data geometry is shown in Fig. 4b. The common-source comparison of the retrieved wavefields to those by PZ summation is shown in Fig. 13a and b. The total wavefield is compared to the recorded pressure field in Fig. 13c. There are slight mismatches in terms of amplitude seen in the far-offset. The zero-lateral-offset comparison is shown in Fig. 14. We see that the match of the downgoing field is better than the full-offset comparison in Fig. 13a. In this zero-later-offset case, the limited aperture in the surface data does not have a big impact since the medium is mostly horizontally layered and the correct initial focusing wavefield is used.

3.3. Vertical borehole

The third example is a standard VSP configuration with 69 receivers in a vertical borehole at $x_1 = 3000$ m. The depth of the receivers is from $x_3 = 500$ m to $x_3 = 1200$ m with a 25 m interval, as shown in Fig. 4c. The retrieved one-way wavefields are compared to those by PZ summation in Fig. 16 and to those by *f-k* dip filtering in Fig. 17. The *f-k* dip filtering is added as it is a standard technique for VSPs and it also only requires single-component data. The figure shows the retrieved up- and downgoing fields for a common source at $x_1 = 3000$ m at the surface. The retrieved total wavefield is compared to the recorded pressure field in Fig. 15. Although minor mismatch can be obversed, the result shows that all three methods works well in retrieving the up- and downgoing wavefields, while all three methods are derived from different point of views.

4. Discussion

Up-down separation of borehole data is a routine process. By comparing our results with those by PZ summation and *f-k* filtering, we show that all three methods retrieves the up- and downgoing fields, although they start from very different point of views. Second, we show that it is possible to retrieve these fields using only single-component data and no prior medium parameter information for any well geometry.

There are several aspects of this method to be mentioned. First, it is derived for a lossless inhomogeneous medium with mildly curved surfaces. Attenuation is considered in the work by Slob et al. (2016). Second, although the method does not require a receiver array in the borehole, it does require a full set of surface reflection responses. A large source-receiver aperture at the surface is necessary for complex medium. More importantly, as the scheme is presented, source signal deconvolution and surface multiple removed are assumed in the surface data. A perfect source signal deconvolution which results in a flat amplitude spectrum would be a challenge in practice. For including the surface multiples, Singh et al. (2017), Ravasi (2017) and Staring et al.

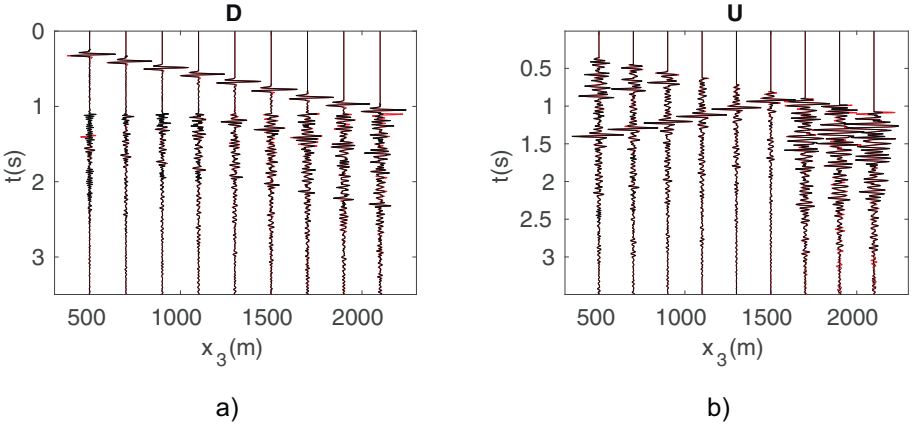

Fig. 17. Vertical borehole case. Similar comparison as in Fig. 16, but to those by *f-k* filtering (in red). (For interpretation of the references to colour in this figure legend, the reader is referred to the web version of this article.)

(2017) show promising results. Nevertheless, we identify that an errornous initial estimate of the focusing wavefield, in terms of amplitude, does not have a major effect on the retrieved the one-way wavefields, especially the upgoing fields. Therefore, this is encouraging news for using borehole data with the Marchenko method.

The fact that only single-component data are needed and that they need not be acquired simultaneously suggests that the method might be suitable for large scale subsurface monitoring (CO_2 monitoring, for example), where the surface data are already available and no major changes happen in the overburden (above a borehole). In particular, the direct arrivals in borehole DAS (Distributed Acoustic Sensing) recording should be considered (Cui et al., 2017), as it is essentially single-component and low-cost for installing in a wide range of boreholes. The proposed method might work well with DAS data for monitoring projects (Daley et al., 2013; Madsen et al., 2013).

5. Conclusion

We show a new approach to retrieve the up- and downgoing fields in boreholes using surface reflection responses. The method is based on the Marchenko method and requires only the acoustic pressure measured at the surface and in boreholes. It is completely data-driven and applicable to any borehole geometry. No receiver array is required, but a full set of surface reflection response is needed. The retrieved one-way wavefield agrees with those by conventional PZ summation and *f-k* filtering. We also observe that the use of only traveltimes from borehole data does not have a major impact on the result (especially the upgoing fields), such that the method is robust. Although practical issues remain for full-scale field application, we believe that the concept of combining surface and borehole data (DAS technology in particular) might be of interest for large scale monitoring projects.

Acknowledgements

The first author would like to acknowledge the sponsors of the DEMODAS project and the ROSE consortium at NTNU for financial support. We thank Jan Thorbecke at TUD for the Open Source modelling package, and Alexander Kritski at Statoil for the velocity model. We thank the reviewers and associate editors for their constructive comments.

References

Amundsen, L., 1993. Wavenumber-based filtering of marine point-source data. Geophysics 58 (9), 1335–1348.
Amundsen, L., Reitan, A., 1995. Decomposition of multicomponent sea-floor data into upgoing and downgoing P- and S-waves. Geophysics 60 (2), 563–572.
Balch, A.H., Lee, M.W., Miller, J.J., Ryder, R.T., 1982. The use of vertical seismic profiles in seismic investigations of the Earth. Geophysics 47 (6), 906–918.
Barr, F.J., Sanders, J.I., 1989. Attenuation of water-column reverbrations using pressure and velocity detectors in a water-bottom cable: Attenuation of water-column reverbrations using pressure and velocity detectors in a water-bottom cable. SEG Technical Program Expanded Abstracts, pp. 653–656.
Behura, J., Wapenaar, K., Snieder, R., 2014. Autofocus imaging: Image reconstruction based on inverse scattering theory. Geophysics 79 (3), A19–A26.
Broggini, F., Snieder, R., Wapenaar, K., 2012. Focusing the wavefield inside an unknown 1D medium: Beyond seismic interferometry. Geophysics 77 (5), A25–A28.
Cui, T., Vasconcelos, I., Rickett, J., Williams, M., 2017. Marchenko redatuming of the Hdvs signal: Marchenko redatuming of the Hdvs signal. 79th EAGE Conference and Exhibition. 2017.
Daley, T.M., Freifeld, B.M., Ajo-Franklin, J., Dou, S., Pevzner, R., Shulakova, V., Kashikar, S., Miller, D.E., Goetz, J., Henninges, J., Lueth, S., 2013. Field testing of fiber-optic distributed acoustic sensing (DAS) for subsurface seismic monitoring. Lead. Edge 32 (6), 699–706.
Dankbaar, J.W.M., 1985. Separation of P- and S-waves: Geophysical Prospecting. 33 pp. 970–986.
Embree, P., Burg, J.P., Backus, M.M., 1963. Wide-band velocity filtering - The pie slice process. Geophysics 28 (6), 948–974.
Hardage, B.A., 1985. Vertical Seismic Profiling, Part A: Principles. Geophysical Press.
Kennett, P., Ireson, Conn, P., 1980. Vertical seismic profiles: Their applications in exploration geophysics. Geophys. Prospect. 28 (5), 676–699.
Madsen, K.N., Dümmong, S., Kritski, A., Finfer, D., Gillies, A., Travis, P., 2013. Simultaneous Multiwell VSP Using Distributed Acoustic Sensing: EAGE (Extended Abstract).
Moon, W., Carswell, A., Tang, R., C., D., 1986. Radon transform wavefield separation for vertical seismic profiling data. Geophysics 51 (4), 940–947.
Muijs, R., Holliger, K., Robertsson, J.O.A., 2004. Data-driven adaptive decomposition of multicomponent seabed recordings. Geophysics 69 (5), 1329–1337.
Poletto, F., Malusa, M., Miranda, F., Tinivella, U., 2004. Seismic while drilling by using dual sensors in drill strings. Geophysics 69 (5), 1261–1271.
Ravasi, M., 2017. Rayleigh-Marchenko redatuming for target-oriented, true-amplitude imaging. Geophysics 82 (6), S439–S452.
de Ridder, S., Curtis, A., van der Neut, J., Wapenaar, K., 2016. Marchenko wavefield redatuming, imaging conditions, and the effect of model errors. SEG Technical Program Expanded Abstracts. 2016, pp. 5155–5159.
Rose, J.H., 2002. Vertical seismic profiles: Their applications in exploration geophysics. 18 (6), 1923.
Schalkwijk, K.M., Wapenaar, C., Verschuur, D.J., 2003. Adaptive decomposition of multicomponent ocean-bottom seismic data into downgoing and upgoing P- and S-waves. Geophysics 68 (3), 1091–1102.
Singh, S., Snieder, R., van der Neut, J., Thorbecke, J., Slob, E., Wapenaar, K., 2017. Accounting for free-surface multiples in Marchenko imaging. Geophysics 82 (1), R19–R30.
Slob, E., Wapenaar, K., Broggini, F., Snieder, R., 2014. Seismic reflector imaging using internal multiples with Marchenko-type equations. Geophysics 79 (2), S63–S76.
Slob, E., Wapenaar, C., Thorbecke, J., 2016. Marchenko equations for acoustic Green's function retrieval and imaging in dissipative media. SEG Technical Program Expanded Abstracts. 2016, pp. 5160–5165.
Staring, M., Grobbe, N., van der Neut, J., Wapenaar, K., 2017. Sparse Inversion for Solving the Coupled Marchenko Equations Including Free-Surface Multiples: 79th EAGE Conference and Exhibition.
Thorbecke, J., Draganov, D., 2011. Finite-difference modeling experiments for seismic interferometry. Geophysics 76 (6), H1–H18.
Thorbecke, J., van der Neut, J., Wapenaar, K., 2013. Green's function retrieval with Marchenko equations: a sensitivity analysis. SEG Technical Program Expanded Abstracts. 2013, pp. 3888–3893.
Thorbecke, J., Slob, E., Brackenhoff, J., van der Neut, J., Wapenaar, K., 2017. Implementation of the marchenko method. Geophysics 82 (6), WB29–WB45.
Treitel, S., Shanks, J.L., Frazier, C.W., 1967. Some aspects of fan filtering. Geophysics 32 (5), 789–798.
Ursin, B., 1983. Review of elastic and electromagnetic wave propagation in horizontally layered media. Geophysics 48 (8), 1063–1081.
Wapenaar, C.P.A., Herrmann, P., Verschuur, D.J., Berkhout, A.J., 1990. Decomposition of multicomponent seismic data into primary P- and S-wave responses. Geophys. Prospect. 38 (6), 633–662.
Wapenaar, K., Broggini, F., Slob, E., Snieder, R., 2013. Three-dimensional single-sided Marchenko inverse scattering, data-driven focusing, Green's function retrieval, and their mutual relations. Phys. Rev. Lett. 110 (8), 084301.
Wapenaar, K., Thorbecke, J., van der Neut, J., Broggini, F., Slob, E., Snieder, R., 2014. Marchenko imaging. Geophysics 79 (3), WA39–WA57.